Ultrafast Electron Correlations and Memory Effects at Work: Femtosecond Demagnetization in Ni

Shree Ram Acharya,[1] Volodymyr Turkowski,[1,*] G. P. Zhang,[2] and Talat S. Rahman[1]
[1]Department of Physics, University of Central Florida, Orlando, Florida 32816, USA
[2]Department of Physics, Indiana State University, Terre Haute, Indiana 47809, USA

(Received 13 November 2019; revised 4 May 2020; accepted 1 June 2020; published 30 June 2020)

Experimental observations of the ultrafast (less than 50 fs) demagnetization of Ni have so far defied theoretical explanations particularly since its spin-flipping time is much less than that resulting from spin-orbit and electron-lattice interactions. Through the application of an approach that benefits from spin-flip time-dependent density-functional theory and dynamical mean-field theory, we show that proper inclusion of electron correlations and memory (time dependence of electron-electron interaction) effects leads to demagnetization at the femtosecond scale, in good agreement with experimental observations. Furthermore, our calculations reveal that this ultrafast demagnetization results mainly from spin-flip transitions from occupied to unoccupied orbitals implying a dynamical reduction of exchange splitting. These conclusions are found to be valid for a wide range of laser pulse amplitudes. They also pave the way for *ab initio* investigations of ultrafast charge and spin dynamics in a variety of quantum materials in which electron correlations may play a definitive role.

DOI: 10.1103/PhysRevLett.125.017202

Introduction.—Ultrafast tuning of the magnetization in transition-metal ferromagnets by short laser pulses has attracted worldwide attention because of possible applications in ultrafast data storage, switches, and spintronics, to name a few. The unusual physical effects accompanying such a fast—femtosecond (fs)—demagnetization, namely, nontrivial dynamics of electrons, spins and lattice, and their interactions (e.g., orbital momentum transfer between the subsystems) have also challenged standard theoretical explanations (see, e.g., Ref. [1]). Beginning with the pioneering observations of Beaurepaire *et al.* on nickel [2], which displayed a large demagnetization when excited by an ultrashort laser pulse, the subject continues to be examined both experimentally and theoretically. Experimental observations [2–11] have now confirmed that this laser-induced demagnetization in Ni bulk and thin films takes place at the subpicosecond regime. The latest results show the timescale to be about 20 fs [11]. Unsurprisingly most theoretical studies have attempted to trace the origin of this demagnetization to intricacies in the electronic and spin structure of the system. Probably the simplest is the phenomenological three-temperature ($3T$) model [2], in which magnetization dynamics is characterized by an effective spin temperature, which equilibrates through energy exchange between the spin subsystem and electron and phonon baths. This model has been used to fit experimentally measured electron and spin temperatures, but it does not provide a microscopic understanding of the processes involved in the demagnetization, except for the possible role of phonons, which occurs at the post picosecond stage. A modified $3T$ model that adds electron-phonon momentum scattering events [12] and another that includes dynamical feedback exchange splitting between majority and minority bands [13] have also been proposed. Efforts have also been made to augment traditional spin wave theory with laser-induced spin-orbit torque to explain the recent observations of ultrafast spin decoherence in Ni [10]. Other proposed mechanisms of demagnetization include superdiffusive spin transport [14] and collective excitation [15] scenarios.

Since phonons and other "slow" effects may not play a large role at femtoseconds, Zhang *et al.* [16] analyzed a model Hubbard Hamiltonian that related the demagnetization to a combined effect of the external laser field and spin-orbit coupling—a conclusion later corroborated experimentally [9]. These Hubbard-model based studies (see Ref. [16] and references therein) have also aimed at understanding the role of electron correlations in the demagnetization but the interaction parameters (fitted to spectroscopic data) used in these studies are quite different from those that provide good agreement with experimental data on the Ni Curie temperature and high-temperature magnetic moment [17].

Ab initio approaches ranging from rigid band density functional theory (DFT) [18] to time-dependent spin DFT [19,20] have also had some success. A TDDFT study [20] based on noncollinear local spin density exchange-correlation (XC) potential with no memory dependence did demonstrate a large decrease of Ni magnetic moment (∼43%) within a few dozen fs, as a result of spin-orbit interactions between the excited and ground state electrons. However, the pulse fluence used [20] were 2 orders of magnitude larger and the pulse wavelength about one-tenth

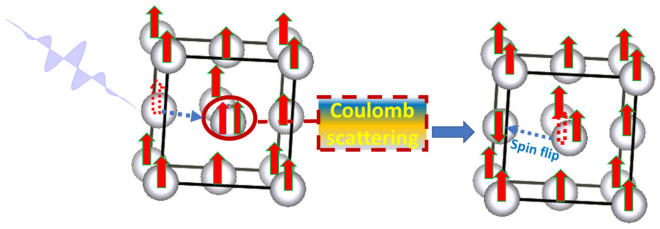

FIG. 1. Schematic representation of Coulomb repulsion induced spin-flip processes in Ni upon perturbation by a laser pulse that results in ultrafast demagnetization of the system.

of those in experiments. On the other hand, incorporation of the time-dependent Liouville equation into DFT [19] with rescaled spin-polarized local density approximation (LDA) and a time-dependent attenuation factor found 10% decrease of magnetic moment for experimentally relevant pulse parameters [19]. Although the demagnetization is much less than in experiments, this study [19] points to the importance of memory effects in XC potentials. Motivated by the above suggestions of interplay of electron correlations and memory effects in ultrafast demagnetization, we present a theoretical model in which we incorporate non-Markovian dynamics in noncollinear spin-density TDDFT [21,22] with the XC kernel derived from dynamical mean-field theory (DMFT) [23,24] based on a Hubbard model suitable for transition metals with partially filled d orbitals. Apart from inherent inclusion of memory effects [25,26], the approach tracks electron correlations at timescale during which lattice effects may be neglected: the first (0–20 fs) of ultrafast spin dynamics in Ni.

Note that such a noncollinear theory would allow spins to flip (Fig. 1) without requiring conservation of S_z, since the magnetization direction varies in space and the z component of spin is not a good (global) quantum number. Realization of such systems includes the helical spin-wave ground state for γ-Fe [27] and systems with varying surface magnetization. One could also visualize a scenario in which the ground state constitutes collinear spins but coupling of the spin-up and spin-down densities, either through an external transverse magnetic perturbation or a spatially dependent effective magnetic field generated by reorientation of the magnetic moments, leads to noncollinearity.

Computational details.—First, we perform spin-polarized DFT [28,29] calculations using the QUANTUM ESPRESSO code [30] to obtain spin-resolved orbital density of states (DOS) and corresponding Kohn-Sham eigenfunctions. The Perdew-Burke-Ernzerhof (PBE) functional [31] under the generalized gradient approximation (GGA) is used to describe the electronic exchange-correlation contribution to the total energy. The valence electron ($4s^2\ 3d^8$) wave functions are expanded using a plane-wave basis with kinetic energy cutoff of 35 Ry and scalar-relativistic, ultrasoft pseudopotential is used to describe core electrons and the nuclei. The bulk Ni Brillouin zone is represented by the Monkhorst-Pack k-point scheme [32] with a $15 \times 15 \times 15$ grid mesh. The structure is ionically relaxed such that forces on an atom converge within 10^{-3} Ry/Å and the total energy within 10^{-4} Ry. The calculated lattice constant of 3.52 Å agrees well with experiments [33]. In the postprocessing calculations of the DOS, $30 \times 30 \times 30$ k points and 20 bands are used.

For the effective Hubbard Hamiltonian solved within DMFT, we choose the local Coulomb repulsion $U = 3.0$ eV and the exchange energy $J = 0.9$ eV obtained by constrained DFT [34], which successfully reproduces several experimental features of Ni [17,35]. To solve DMFT equations in the Matsubara (imaginary) frequency representation with discrete fermionic frequencies $i\omega_n = i\pi T(2n+1)$, we take $n = 250$, $k_B T = 0.01$ eV and use the multiorbital iterative perturbation theory (MO-IPT) approximation [36] (details in the Supplemental Material [37], Sec. I) which reproduces the main features of the DMFT solution and is computationally less demanding than the state of the art continuous-time quantum Monte Carlo solver [38]. The obtained Green's function is then transformed into the real frequency representation through the Pade approximation [39]. With the above parameters, we obtain Ni Curie temperature $T_c \approx 627$ K, in good agreement with 631 K found in experiments [33]. Although this agreement may be fortuitous, it indicates that the chosen U and J values are not unrealistic.

To simulate electron dynamics, we use spin-flip TDDFT Kohn-Sham equations for the spin wave functions, whose general form is

$$\left[\left(-\frac{\nabla^2}{2m} + V_H[n](\mathbf{r},t)\right)\delta_{\sigma\sigma'} + V_{\mathrm{XC}\sigma\sigma'}[n](\mathbf{r},t) + V_{\mathrm{ext}\sigma\sigma'}(\mathbf{r},t)\right]$$
$$\Psi_{k\sigma'}(\mathbf{r},t) = i\frac{\partial \Psi_{k\sigma}(\mathbf{r},t)}{\partial t}, \tag{1}$$

where $-\nabla^2/2m$ is the kinetic energy operator, $V_H[n](\mathbf{r},t) = \int [n(\mathbf{r}',t)/|\mathbf{r}-\mathbf{r}'|]\mathrm{d}\mathbf{r}'$ is the Hartree potential, $V_{\mathrm{XC}\sigma\sigma'}[n](\mathbf{r},t)$ is the XC potential matrix, σ refers to spin indices, and $V_{\mathrm{ext}\sigma\sigma'}(\mathbf{r},t)$ is the external potential. Here $V_{\mathrm{XC}\sigma\sigma'}[n](\mathbf{r},t)$ is a functional of the spin-density matrix

$$n_{\sigma\sigma'}(\mathbf{r},t) = \sum_{k\le k_F} \Psi_{k\sigma}(\mathbf{r},t)\Psi^*_{k\sigma'}(\mathbf{r},t), \tag{2}$$

and $V_{\mathrm{ext}\sigma\sigma'}(\mathbf{r},t)$ represents the laser pulse field which in the dipole approximation is $\delta_{\sigma\sigma'} e\mathbf{r}.\mathbf{E}(t)$ (valid since the pulse wavelength is longer than the lattice parameters). The external electric field is taken as $\boldsymbol{E}(t) = E_0 e^{-t^2/\tau^2}\cos(\omega t)(\hat{x}+\hat{y}+\hat{z})$, where E_0, τ, ω, $\hat{x}$, $\hat{y}$, and $\hat{z}$ are the electric field amplitude, the pulse duration, the field frequency and the unit vectors along x, y, and z-directions, respectively. Unless specified otherwise, in this work E_0 and $\hbar\omega$ are 0.05 V/Å and 2 eV, as in the TDLDA study [18], whereas τ is taken to be 7.2 fs, slightly less than previously used [18].

Using linear response, the XC potential in Eq. (1) can be expressed in terms of XC kernel matrix $f_{\mathrm{XC}\sigma\sigma'\bar{\sigma}\bar{\sigma}'}(\mathbf{r},t,\mathbf{r}',t')$ as

$$V_{\mathrm{XC}\sigma\sigma'}[n](\mathbf{r},t) = V_{\mathrm{XC}\sigma\sigma'}[n](\mathbf{r},t=0) + \sum_{\bar{\sigma},\bar{\sigma}'}\int f_{\mathrm{XC}\sigma\sigma'\bar{\sigma}\bar{\sigma}'}(\mathbf{r},t,\mathbf{r}',t')\delta n_{\bar{\sigma}\bar{\sigma}'}(\mathbf{r}',t')d\mathbf{r}'dt', \quad (3)$$

where $V_{\mathrm{XC}\sigma\sigma'}[n](\mathbf{r},t=0)$ is the static or DFT part of the XC potential and

$$f_{\mathrm{XC}\sigma\sigma'\bar{\sigma}\bar{\sigma}'}(\mathbf{r},t,\mathbf{r}',t') = \frac{\delta V_{\mathrm{XC}\sigma\sigma'}[n](\mathbf{r},t)}{\delta n_{\bar{\sigma}\bar{\sigma}'}(\mathbf{r}',t')}. \quad (4)$$

In the DMFT approximation, $f_{\mathrm{XC}\sigma\sigma'\bar{\sigma}\bar{\sigma}'}(\mathbf{r},t,\mathbf{r}',t')$ becomes the product of the space- and time-dependent parts

$$f_{\mathrm{XC}\sigma\sigma'\bar{\sigma}\bar{\sigma}'}(\mathbf{r},\mathbf{r}',t,t') = \delta(\mathbf{r}-\mathbf{r}')f^{\mathrm{DMFT}}_{\mathrm{XC}\sigma\sigma'\bar{\sigma}\bar{\sigma}'}(t-t'), \quad (5)$$

where $f^{\mathrm{DMFT}}_{\mathrm{XC}\sigma\sigma'\bar{\sigma}\bar{\sigma}'}(t-t')$ is obtained from Fourier transform of the frequency-dependent term $f^{\mathrm{DMFT}}_{\mathrm{XC}\sigma''\sigma'''\bar{\sigma}''\bar{\sigma}'''}(\omega)$ that satisfies the equation

$$\chi_{\alpha\beta}(\omega) = \chi^{(0)}_{\alpha\beta}(\omega) + \sum_{\gamma,\delta}\chi^{(0)}_{\alpha\gamma}(\omega)f^{\mathrm{DMFT}}_{\mathrm{XC}\gamma\delta}(\omega)\chi_{\delta\beta}(\omega). \quad (6)$$

In Eq. (6), to simplify notation we express the XC kernel and other matrices (defined below) in the form of a 4×4 matrix whose rows (columns) are defined by pairs of the following indices: $1=\uparrow\uparrow$, $2=\uparrow\downarrow$, $3=\downarrow\uparrow$, and $4=\downarrow\downarrow$. The other matrices in Eq. (6) are the Fourier transform of the correlation function (generalized susceptibility) $\chi_{\sigma\sigma'\bar{\sigma}\bar{\sigma}'}(t) = -\sum_{a,b}\langle\hat{T}c^{a+}_{\sigma}(t)c^{a}_{\sigma'}(t)c^{b+}_{\bar{\sigma}}(0)c^{b}_{\bar{\sigma}'}(0)\rangle$ [$\chi^{(0)}_{\sigma\sigma'\bar{\sigma}\bar{\sigma}'}(\omega)$ for the noninteracting case], where c^{a}_{σ} and c^{a+}_{σ} are the electron annihilation and creation operators, respectively, a, b are band indices, and $\hat{T}$ is the time-ordering operator (for details see Supplemental Material [37], Sec. II).

After we calculate the susceptibility within DMFT, we substitute it into Eq. (6) to obtain the following XC kernel matrix after matrix inversion:

$$\hat{f}^{\mathrm{DMFT}}_{\mathrm{XC}}(\omega) = \begin{pmatrix} f_{\mathrm{XC11}}(\omega) & 0 & 0 & 0 \\ 0 & 0 & f_{\mathrm{XC23}}(\omega) & 0 \\ 0 & f_{\mathrm{XC32}}(\omega) & 0 & 0 \\ 0 & 0 & 0 & f_{\mathrm{XC44}}(\omega) \end{pmatrix}. \quad (7)$$

Substitution of the time domain transformation of the above matrix in Eq. (3) yields the XC potential. The nondiagonal elements of Eq. (7) represent spin-flip processes: for example, $f_{\mathrm{XC32}}(\omega)$ accounts for spin-up to spin-down transition. Furthermore, the limiting case of "no-memory" solution of the problem is obtained by approximating the XC kernel $\hat{f}^{\mathrm{DMFT}}_{\mathrm{XC}}(\omega) = \hat{f}^{\mathrm{DMFT}}_{\mathrm{XC}}(0)$, which in the real time representation becomes

$$f_{\mathrm{XC}\sigma\sigma'\bar{\sigma}\bar{\sigma}'}(\mathbf{r},\mathbf{r}',t,t') = \delta(\mathbf{r}-\mathbf{r}')f^{\mathrm{DMFT}}_{\mathrm{XC}\sigma\sigma'\bar{\sigma}\bar{\sigma}'}(0)\delta(t-t'). \quad (8)$$

Finally, the Kohn-Sham equation [Eq. (1)] is solved using the density-matrix formalism in which the time-dependent density matrix elements $\rho^{\mathrm{ln}}_{k\sigma\sigma'}(t)$ are calculated by propagating the Liouville equation $i[\partial\rho^{\mathrm{ln}}_{k\sigma\sigma'}(t)/\partial t] = [H,\rho]^{\mathrm{ln}}_{k\sigma\sigma'}(t)$, where $H^{\mathrm{nl}}_{k\sigma\sigma'}(t) = \int\psi^{n^*}_{k\sigma}(\mathbf{r})\hat{H}_{\sigma\sigma'}(\mathbf{r},t)\psi^{l}_{k\sigma'}(r)d\mathbf{r}$ are the time independent orbital-spin matrix elements of the Hamiltonian $\hat{H}_{\sigma\sigma'}(\mathbf{r},t)$ defined by Eq. (1) (see Supplemental Material [37], Sec. III for details).

A final remark should be made about the angular momentum dynamics of the system. Earlier models assumed possible change of angular momentum of the system due to photon absorption [16]. More popular (see, e.g., Refs. [12,40,41]) is the scenario in which the spin-flip processes are accompanied by transfer of angular momentum to the lattice as a result of electron-phonon scattering. During the after-pulse dynamics, in the absence of electron-phonon scattering, noncollinear coupling may be sufficient to redistribute angular momentum between spin and orbital momenta "subsystems." In the absence of spin-orbit interaction, one may thus expect ultrafast demagnetization driven by electron correlation effects which may lead to a redistribution of the excited electrons from the majority to minority bands [42]. In this work, we consider an electron correlation induced (noncollinear) scenario of ultrafast demagnetization.

Results.—In Fig. 2, we show the TDDFT results for the time dependence of demagnetization in Ni after laser pulse perturbation, using three different XC kernels: (i) with full memory effects; (ii) no memory effects; (iii) memory effects in only the spin-flip part. The first produces

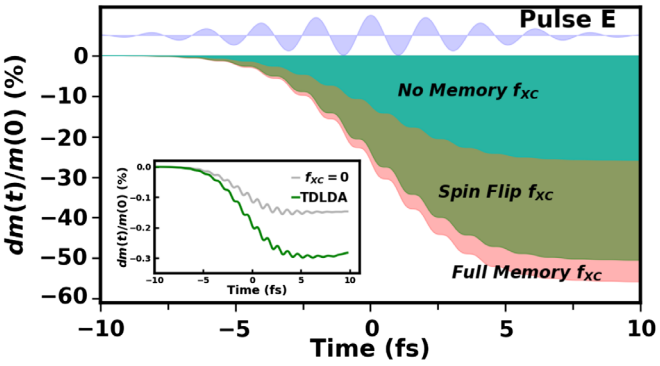

FIG. 2. The demagnetization dynamics, $dm(t)$, calculated from Eq. III. 3 in the Supplemental Material [37] by using XC kernel matrix with full memory dependence, i.e., Eq. (7) (edge of pink shaded area), with no memory dependence, i.e., Eq. (8) (edge of blue shaded area) and with only spin-up to spin-down flip part of the memory dependence, i.e., keeping only f_{XC32} in Eq. (7) nonzero (edge of green shaded area). The amplitude, duration, and frequency of pulse are taken as 0.05 V/Å, 7.2 fs, and $\hbar\omega = 2$ eV, respectively. The dynamics for limiting cases of no f_{XC} and LDA XC in TDDFT is shown in the inset.

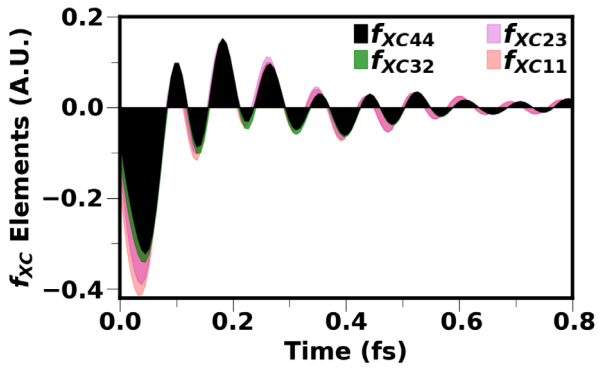

FIG. 3. Time dependence of the nonzero components of the DMFT XC kernel of bulk Ni obtained from the Fourier transform of matrix elements in Eq. (7).

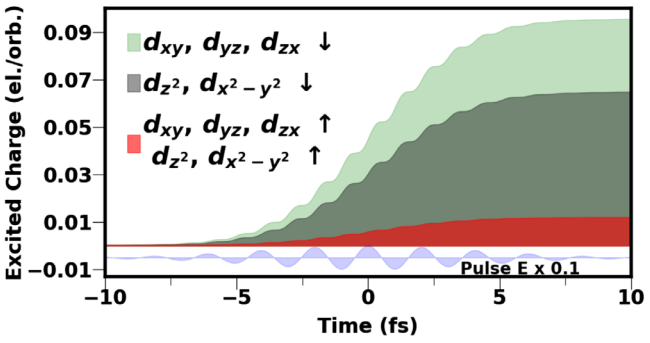

FIG. 4. Orbital and spin resolved dynamics of excited charge obtained as the diagonal elements of the density matrix.

demagnetization of 56% in good agreement with what we extract from experimental data: ∼40% for pulse with $\hbar\omega =$ 2 eV and 7 mJ/cm^2 fluence [2] and ∼70% for pulse of $\hbar\omega = 1.55$ eV and fluence of 7.36 mJ/cm^2 (absorbed fluence of 2.56 mJ/cm^2) [11], while the XC kernel with no memory effects results in about 25.8% demagnetization. This last result is interesting despite being one-half of that obtained with memory effects, as it is much larger than those obtained with standard TDDFT, pointing to the importance of electron correlations which is inherent in our XC kernel. Figure 2 also shows demagnetization of 50.6% when memory effects are confined to the spin-flip part of the XC kernel, indicating that the major channel of demagnetization is spin-up to spin-down transition. To probe further the origin of this enhanced ultrafast effect, we plot in Fig. 3 the time dependence of the matrix elements of the DMFT XC kernel to find that the effect is dramatic only at short times (<0.1 fs), dying out within ∼1 fs, which is of order of electron-electron scattering time in correlated materials.

The inset of Fig. 2 summarizes the demagnetization that we obtain in the limiting case of zero f_{XC} and standard TDLDA. Note that the maximum demagnetization obtained for these cases is about 0.28%, a value close to that obtained in other theoretical studies and far from the experimental results, as summarized in the introduction.

Analyses of the orbital and spin-resolved excited charge dynamics shown in Fig. 4 provide further insight that the population of the excited spin-down electrons is significantly higher than those of spin-up orientation. This result is consistent with the higher density of unoccupied spin-down states near the Fermi energy (E_F) in Fig. 5, which compares the DOS of Ni d states obtained with DFT and DFT + DMFT. Among all spin-down orbitals, the presence of higher excited charge density in the d_{xy}, d_{yz}, and d_{xz} orbitals as compared to the d_{z2}, d_{x2-y2} orbitals is also consistent with their relatively higher DOS near E_F in Fig. 5. The slight shift in the DMFT DOS compared to the DFT solution in Fig. 5 is attributable to local correlation and exchange effects. Note that the change in the magnetic moment per Ni atom is minor: 0.64 μ_B in DFT and 0.61 μ_B in DMFT—a bit closer to the experimental value of 0.57 μ_B [43]. The slight reduction in the magnetic moment in DMFT may be ascribed to small increase in the occupancy of spin-down orbitals. Since the imbalance in the orbital occupancy that contributes to magnetization results mostly from 3d orbitals and since near E_F the d orbitals DOS is significantly higher than that of the p orbitals, especially in the valence band, we have considered contributions of only the d orbitals in the study. It should be noted that the orbital DOS presented in Fig. 5 are not in exact agreement with those in other studies, e.g., in Ref. [44], as a result of differences in the applied DMFT solvers. However, the main features of the total d-electron DOS are similar in all cases: both spin-up and spin-down states are mostly located between −5 eV and E_F, while the predominantly empty spin-down states occupy energies below ∼0.5 eV. Thus, the excited (to a large degree, state-averaged) dynamics of total spin-up and spin-down densities that define the total experimentally observed demagnetization is expected to be similar despite subtle differences in the DOS.

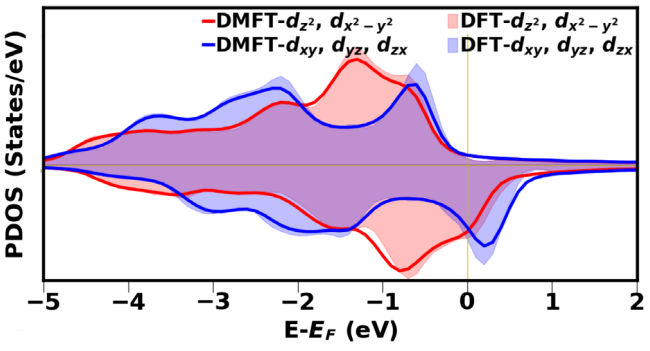

FIG. 5. The projected density of states (PDOS) of bulk Ni obtained using DFT (shaded area) and the spectral function obtained using DFT + DMFT approach (continuous curves) with on-site Coulomb interaction $(U) = 3.0$ eV and exchange interaction $(J) = 0.9$ eV. The PDOS of minority spin is flipped. The majority (minority) PDOS curves are above (below) the yellow horizontal line.

In agreement with experimental results, our calculations show a strong dependence of demagnetization on the pulse field amplitude, i.e., the intensity or fluence [11,12,45], and the demagnetization time increases with amplitude [46] (see Fig. SI. 1 in the Supplemental Material [37], which includes details of demagnetization calculations). Examination of the change of the (m) components and of the total z projection of the angular momentum during the process of demagnetization (Supplemental Material [37], Sec. V) also reveal that change is small (see Fig. SI. 2 in the Supplemental Material [37]), which confirms that spin-flip processes play a dominant role in the demagnetization. We should also emphasize that the demagnetization time depends strongly on the pulse duration. For example, the experimental demagnetization time constants for Ni obtained by Radu and collaborators, ∼120 fs [47], were obtained for pulses much longer (∼60 fs) than those considered by us. Naturally, longer pulses produce more excitations, i.e., they increase the effect of interactions and as a result increase the demagnetization time. Besides, the demagnetization time cannot be shorter than the pulse duration (which is 60 fs in Ref. [47]). Since electron correlations and memory effects are expected to be at the 1–10 fs timescale (rough estimate of electron scattering time from correlations or exchange is $\hbar/U \sim 0.2$ to $\hbar/J \sim 1$ fs, plus the memory time, which we showed earlier to be ∼1 fs), we choose here short pulses that allow examination of the effects with relatively low computational cost. More generally, as our results for demagnetization for different pulse fluences show (Fig. 1 in the Supplemental Material [37]), demagnetization time increases with increasing pump fluence, in agreement with experimental observations (see, e.g., Ref. [11]).

In short, we have demonstrated above that spin-flip processes caused by electron correlations in a noncollinear spin system produces a large demagnetization in Ni at timescales comparable to that experimentally observed ∼50 fs. It is important to stress that the above scenario is valid only for noncollinear spin systems in which spin spatial orientations vary site to site on the lattice. While lattice (phonon) effects may also contribute to the magnetization dynamics in this noncollinear scenario, we expect them to be important at longer times [12].

Conclusions.—In this work, on the basis of spin TDDFT with noncollinear DMFT XC kernel which incorporates time-resolved Coulomb interactions we have provided a theoretical understanding of the experimentally observed large ultrafast demagnetization of Ni by tracing it to spin-flip transitions resulting from electron correlations and memory effects that occur at few fs after perturbation by a laser pulse. In other words, our results suggest that electron correlations, and not photon-orbital momenta, electron-phonon, or other interactions, play the dominant role in femtosecond scale dynamics. The other contributions occur at larger timescales. Conclusions about a definitive role of electron correlations in Ni demagnetization were also drawn recently in a real-time TDDFT analysis [48] with the spin LDA exchange correlation potential and pulses longer than those considered. However, demagnetization times and values comparable to experiments could only be obtained when significant disorder was introduced in the system, unsurprisingly because of limitations of LDA already discussed.

Our results without time-resolved electron-electron interactions also lead to demagnetization, albeit only one-half the observed demagnetization, pointing to the importance of the memory or time or frequency dependence of the kernel. Nevertheless, some questions need further answers for full success of the present DMFT inspired TDDFT framework, the most important of which are the nonlinear response (requiring approximation beyond the XC kernel) and the longer-time dynamics, at which point phonon scattering becomes important. These are topics for future investigations. The *ab initio* framework provided here should pave the way for applications to other magnetic systems including iron and cobalt, for which we expect a similar behavior due to similarities in their density of states and local Coulomb repulsion energies. Understanding of the combined role of electron correlations, spin-orbit interactions, phonon mediated spin interactions, would eventually help obtain the design principles for ultrafast magnetic technologies.

We thank Carsten Ulrich for many helpful discussions and acknowledge computational resources provided by the STOKES facility at the University of Central Florida. This work was partially supported by U.S. DOE Grant No. DE-FG02-07ER46354 (S. R. A., V. T., and T. S. R.) and Grant No. DE-FG02-06ER46304 (G. P. Z.). We dedicate this work to the memory of Eric Beaurepaire and Jean-Yves Bigot whose seminal works and beautiful writings inspired our efforts. The authors declare no competing financial interests.

*To whom all correspondence should be addressed.
Volodymyr.Turkowski@ucf.edu

[1] A. Kirilyuk, A. V. Kimel, and Th. Rasing, Rev. Mod. Phys. **82**, 2731 (2010).
[2] E. Beaurepaire, J.-C. Merle, A. Daunois, and J.-Y. Bigot, Phys. Rev. Lett. **76**, 4250 (1996).
[3] J. Hohlfeld, E. Matthias, R. Knorren, and K. H. Bennemann, Phys. Rev. Lett. **78**, 4861 (1997).
[4] A. Scholl, L. Baumgarten, R. Jacquemin, and W. Eberhardt, Phys. Rev. Lett. **79**, 5146 (1997).
[5] J. Güdde, U. Conrad, V. Jähnke, J. Hohlfeld, and E. Matthias, Phys. Rev. B **59**, R6608 (1999).
[6] H.-S. Rhie, H. A. Dürr, and W. Eberhardt, Phys. Rev. Lett. **90**, 247201 (2003).
[7] M. Lisowski, P. A. Loukakos, A. Melnikov, I. Radu, L. Ungureanu, M. Wolf, and U. Bovensiepen, Phys. Rev. Lett. **95**, 137402 (2005).
[8] C. Stamm *et al.*, Nat. Mater. **6**, 740 (2007).

[9] J.-Y. Bigot, M. Vomir, and E. Beaurepaire, Nat. Phys. **5**, 515 (2009).
[10] P. Tengdin *et al.*, Sci. Adv. **4**, eaap9744 (2018).
[11] W. You *et al.*, Phys. Rev. Lett. **121**, 077204 (2018).
[12] B. Koopmans, G. Malinowski, F. Dalla Longa, D. Steiauf, M. Fähnle, T. Roth, M. Cinchetti, and M. Aeschlimann, Nat. Mater. **9**, 259 (2010).
[13] B. Y. Mueller, A. Baral, S. Vollmar, M. Cinchetti, M. Aeschlimann, H. C. Schneider, and B. Rethfeld, Phys. Rev. Lett. **111**, 167204 (2013).
[14] M. Battiato, K. Carva, and P. M. Oppeneer, Phys. Rev. Lett. **105**, 027203 (2010).
[15] T. Ostler *et al.*, Nat. Commun. **3**, 666 (2012).
[16] G. P. Zhang and W. Hübner, Phys. Rev. Lett. **85**, 3025 (2000).
[17] A. I. Lichtenstein, M. I. Katsnelson, and G. Kotliar, Phys. Rev. Lett. **87**, 067205 (2001).
[18] G. P. Zhang, Y. Bai, W. Hübner, G. Lefkidis, and T. F. George, J. Appl. Phys. **103**, 07B113 (2008).
[19] G. P. Zhang, Y. Bai, and T. F. George, J. Phys. Condens. Matter **28**, 236004 (2016).
[20] K. Krieger, J. Dewhurst, P. Elliott, S. Sharma, and E. Gross, J. Chem. Theory Comput. **11**, 4870 (2015).
[21] Y. Shao, M. Head-Gordon, and A. I. Krylov, J. Chem. Phys. **118**, 4807 (2003).
[22] J. Gao, W. Liu, B. Song, and C. Liu, J. Chem. Phys. **121**, 6658 (2004).
[23] W. Metzner and D. Vollhardt, Phys. Rev. Lett. **62**, 324 (1989).
[24] A. Georges, G. Kotliar, W. Krauth, and M. J. Rozenberg, Rev. Mod. Phys. **68**, 13 (1996).
[25] V. Turkowski and T. S. Rahman, J. Phys. Condens. Matter **29**, 455601 (2017).
[26] S. R. Acharya, V. Turkowski, and T. S. Rahman, Computation **4**, 34 (2016).
[27] E. Sjöstedt and L. Nordström, Phys. Rev. B **66**, 014447 (2002).
[28] P. Hohenberg and W. Kohn, Phys. Rev. **136**, B864 (1964).
[29] W. Kohn and L. J. Sham, Phys. Rev. **140**, A1133 (1965).
[30] P. Giannozzi *et al.*, J. Phys. Condens. Matter **21**, 395502 (2009).
[31] J. P. Perdew, K. Burke, and M. Ernzerhof, Phys. Rev. Lett. **77**, 3865 (1996).
[32] H. J. Monkhorst and J. D. Pack, Phys. Rev. B **13**, 5188 (1976).
[33] H. Landolt and R. Börnstein, *Numerical Data and Functional Relationships in Science and Technology: Crystal and Solid State Physics,* New Series Group 3 (Springer, New York, 1971), Vol. 5.
[34] T. Bandyopadhyay and D. D. Sarma, Phys. Rev. B **39**, 3517 (1989).
[35] O. Miura and T. Fujiwara, Phys. Rev. B **77**, 195124 (2008).
[36] M. S. Laad, L. Craco, and E. Müller-Hartmann, Phys. Rev. B **73**, 045109 (2006).
[37] See Supplemental Material at http://link.aps.org/supplemental/10.1103/PhysRevLett.125.017202 for further details of the method used, orbitals resolved contribution to demagnetization and the manipulation of demagnetization using external field.
[38] E. Gull, A. J. Millis, A. I. Lichtenstein, A. N. Rubtsov, M. Troyer, and P. Werner, Rev. Mod. Phys. **83**, 349 (2011).
[39] H. Vidberg and J. Serene, J. Low Temp. Phys. **29**, 179 (1977).
[40] C. Dornes *et al.*, Nature (London) **565**, 209 (2019).
[41] M. Hennecke, I. Radu, R. Abrudan, T. Kachel, K. Holldack, R. Mitzner, A. Tsukamoto, and S. Eisebitt, Phys. Rev. Lett. **122**, 157202 (2019).
[42] M. Krauß, T. Roth, S. Alebrand, D. Steil, M. Cinchetti, M. Aeschlimann, and H. C. Schneider, Phys. Rev. B **80**, 180407(R) (2009).
[43] M. Stearns, *Landolt-Börnstein Series* (Springer, Berlin, 1986), p. 45.
[44] A. Hausoel, M. Karolak, E. Şaşıoğlu, A. Lichtenstein, K. Held, A. Katanin, A. Toschi, and G. Sangiovanni, Nat. Commun. **8**, 16062 (2017).
[45] C. La-O-Vorakiat *et al.*, Phys. Rev. X **2**, 011005 (2012).
[46] E. Carpene, E. Mancini, C. Dallera, M. Brenna, E. Puppin, and S. De Silvestri, Phys. Rev. B **78**, 174422 (2008).
[47] I. Radu *et al.*, Spin **5**, 1550004 (2015).
[48] Z. Chen and L.-W. Wang, Sci. Adv. **5**, eaau8000 (2019).